Available online at www.sciencedirect.com
ScienceDirect
Journal of Catalysis 248 (2007) 213–225
JOURNAL OF CATALYSIS
www.elsevier.com/locate/jcat

Microkinetic modeling of nitrous oxide decomposition on dinuclear oxygen bridged iron sites in Fe-ZSM-5

Niels Hansen [a,*], Andreas Heyden [b,*], Alexis T. Bell [c,*], Frerich J. Keil [a]

[a] *Department of Chemical Engineering, Hamburg University of Technology, D-21073 Hamburg, Germany*
[b] *Department of Chemistry, University of Minnesota, Minneapolis, MN 55455-0431, USA*
[c] *Department of Chemical Engineering, University of California, Berkeley, CA 94720-1462, USA*

Received 11 January 2007; revised 10 March 2007; accepted 15 March 2007

Available online 24 April 2007

Dedicated to Prof. Bernhard Lücke on the occasion of his 70th birthday

Abstract

The decomposition of N_2O on dinuclear oxygen-bridged iron sites in Fe-ZSM-5 was simulated under steady-state conditions considering the reaction mechanism and the rate parameters proposed by Hansen et al. [J. Phys. Chem. C 111 (2007) 2092] on the basis of DFT calculations. The presence of low concentrations of water vapor in the feed stream (ppb to ppm levels) affects the calculated values for the apparent activation energy and the pre-exponential factor and thus can explain the wide variation in experimental values for these quantities, as well as the appearance of an apparent compensation effect. The activity of the dinuclear oxygen-bridged site was compared with that of the mononuclear iron site proposed earlier by Heyden et al. [J. Phys. Chem. B 109 (2005) 1857]; the latter was found to be slightly more active. Microkinetic models for both mononuclear and dinuclear iron sites were used to reproduce temperature-programmed reaction experiments reported for Fe-ZSM-5 samples with low and high iron content. This analysis leads to the conclusion that at very low Fe/Al ratios, mononuclear iron sites prevail, whereas at higher Fe/Al ratios, both mononuclear and dinuclear iron sites are likely to be present simultaneously.

Keywords: N_2O decomposition; Fe-ZSM-5; Microkinetic analysis

1. Introduction

Nitrous oxide (N_2O) is both a greenhouse gas and a contributor to ozone destruction in the stratosphere [1,2]. Reduced emissions of N_2O from adipic acid and nitric acid plants can be achieved by decomposition; zeolites exchanged with 3*d* ions have been shown to be particularly active catalysts for this process [3,4]. Notable among these materials is Fe-ZSM-5, which is able to maintain its activity under industrial tail gas conditions of nitric acid plants [5,6]. Although Fe-ZSM-5 has been extensively studied [7–22], the structure of the active site remains a subject of discussion in the literature [23]. A question of particular interest is the nuclearity of the catalytically active site [11,24–28]. According to a critical evaluation of this subject by Pirngruber et al. [29], many results concerning the nuclearity of the active site published in the past need to be reconsidered due to misinterpretation of experimental data. However, for most Fe-ZSM-5 samples (except those with very low iron content), it is reasonable to assume that a distribution of active iron species exists that depends on the iron content and the catalyst preparation and activation procedures, and that several types of sites differing in iron nuclearity contribute to the observed activity [13,30–32]. Due to this variety of Fe species, the unequivocal assignment of catalytic properties to a single type of iron is difficult by experimental methods alone. In principle, theoretical methods can be used to separate the contribution of an individual species from the total activity of all active species and, thus to investigate the importance of a particular type of site. The capability of mononuclear extra-framework iron sites to catalyze N_2O decomposition in the absence and the presence of NO has been demonstrated recently in two comprehensive

* Corresponding authors.
E-mail addresses: n.hansen@tuhh.de (N. Hansen), heyden.andreas@gmail.com (A. Heyden), bell@cchem.berkeley.edu (A.T. Bell).

0021-9517/$ – see front matter
doi:10.1016/j.jcat.2007.03.015

DFT studies reported by Heyden et al. [33,34]. In a complementary study, Hansen et al. [35] have shown that dinuclear oxygen-bridged extra-framework iron sites are also active for N_2O decomposition and exhibit activation energies for elementary processes involved in N_2O decomposition that are very similar to those determined for mononuclear iron sites. Furthermore, the results of the latter study suggest that larger iron oxide clusters exhibit a very low activity in N_2O decomposition, as was found experimentally [10,28].

The exploration of the reaction mechanism on a specific active site model requires the investigation of all possibly relevant elementary processes on this site. Most often, the resulting reaction mechanism is too complex to allow us to determine which rate processes are most relevant simply by inspecting the magnitude of the rate coefficients for these processes. This difficulty can be overcome by microkinetic modeling, on the basis of which it is possible to determine processes that are most relevant in a complex reaction network and to investigate the influence of rate parameters in a systematic manner [36]. Rate expressions for catalyzed reactions obtained in this way are more likely to offer a good description of the kinetics over a wide range of reaction conditions than those developed empirically, because they are based on an understanding of the reaction mechanism.

The application of this approach to N_2O decomposition on mononuclear iron sites in Fe-ZSM-5 [37] has identified two hidden parameters not described in experimental studies: the fraction of iron sites that are catalytically active and the effect of small partial pressures of H_2O on catalyst deactivation. We demonstrated that these parameters are responsible for the wide variation of values of the apparent pre-exponential factors and activation energies reported in the literature [37].

In the present study, we report a microkinetic model for the mechanism and kinetics of N_2O decomposition occurring on dinuclear, oxygen-bridged extra-framework iron sites in Fe-ZSM-5 [35]. It is the aim of this study to show the influences of the water partial pressure on the catalytic activity of such sites and to demonstrate the similarities in the catalytic properties of these sites to mononuclear iron sites. We also show that microkinetic analysis carried out with mononuclear and dinuclear iron sites can be used to ascertain which type of site is likely to be predominant in a given catalyst. This analysis leads to the conclusion that at very low Fe/Al ratios, mononuclear iron sites prevail, whereas at higher Fe/Al ratios, both mononuclear and dinuclear iron sites are likely to be present simultaneously.

2. Theoretical methods

In earlier work [35] we presented a detailed reaction mechanism for N_2O decomposition on dinuclear iron sites in Fe-ZSM-5, consisting of 39 elementary reactions involving 33 surface species. Activation barriers for each elementary process were determined using density functional theory (DFT). In the present study, equilibrium constants and reaction rate constants were computed using standard methods of statistical mechanics and absolute rate theory [38]. We used the harmonic approximation and included the contributions of the translational, rotational, vibrational, and electronic partition functions of all gaseous species participating in the reaction and the vibrational and electronic contribution of the zeolite cluster. Because the zeolite cluster is part of a solid, translational and rotational partition functions for the zeolite were assumed to be equal in the reactant and transition states. For elementary processes in which the spin state changes during reaction, absolute rate theory was used under the assumption that the partition function of the hypothetical transition state (minimum on the seam of two potential energy surfaces) and the partition function of the minimum state with lower spin multiplicity are identical except for the electronic energy. This procedure completely neglects a low spin-surface crossing probability. To evaluate whether very low spin-surface crossing probabilities could have a significant effect on the reaction rate constants, thermally averaged spin transition probabilities were calculated with the Landau–Zener formula [39] using spin–orbit coupling energies (H_{12}) of 395 and 825 J/mol, as calculated by Danovich and Shaik [40] for the oxidative activation of H_2 by FeO^+. Additional details concerning the calculation of rate parameters and the estimation of errors have been given elsewhere [33,41]. It is important to note that the necessary correction for the reaction rates to account for a spin-inversion probability <1 is comparable to the error inherent in the DFT calculations of activation energies. In addition, the rates of spin-surface crossing were never rate-limiting in this work, and thus spin-surface crossing should not influence the overall kinetics of the reaction network studied.

In our preceding contribution [35], we demonstrated that antiferromagnetic coupling of the two iron atoms has no significant effect on the reaction mechanism. Moreover, others have shown experimentally that the strength of antiferromagnetic coupling decreases with increasing temperature [29]. Therefore, unless stated otherwise, all simulated results were obtained using the reaction rates determined for ferromagnetically coupled iron atoms. The results of all quantum chemical and statistical mechanics calculations are summarized in Tables 1–3 in Appendix A. The order in which the reactions are listed in Table 1 is related to the description of the catalytic cycles in our earlier paper [35].

For a fixed gas composition and temperature, the steady-state material balance for surface species can be written as a set of linear equations that can be readily solved using standard methods [42–44]. Simulations carried out with the entire reaction network reported by Hansen et al. [35] revealed that most processes do not contribute significantly to the overall kinetics, and the reaction mechanism shown in Fig. 1 is sufficient.

3. Results and discussion

3.1. Effects of water vapor on the catalyst surface and the apparent rate constant

In our previous study [35], we showed that desorption of water from dinuclear, oxygen-bridged iron sites is strongly endothermic. Consequently, water vapor decreases the rate constant and has a strong influence on the distribution of dinuclear iron sites among the species $Z^-[HOFeOFeOH]^{2+}Z^-$,

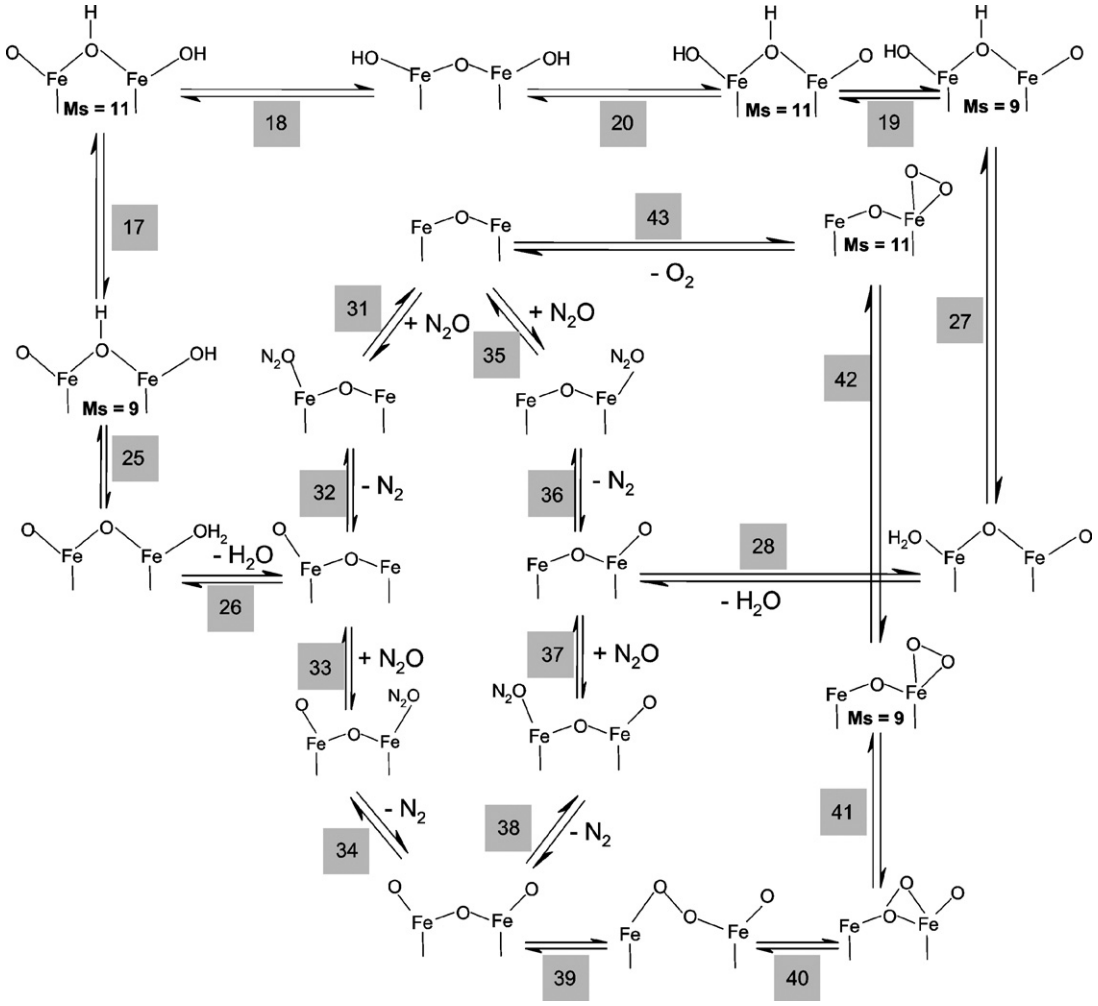

Fig. 1. Reaction network of the N_2O dissociation on dinuclear oxygen-bridged extraframework iron sites in Fe-ZSM-5. For elementary steps which involve spin surface crossing the spin multiplicities of the reactant and product state are specified. The reaction numbers refer to Table 1.

$Z^-[OFeOFe]^{2+}Z^-$, $Z^-[FeOFeO]^{2+}Z^-$, and $Z^-[FeOFe]^{2+}Z^-$. Fig. 2 shows the effects of water on the distribution of the most abundant surface species at 600 and 700 K. At the higher temperature, traces of water have very little effect on the distribution of the catalytically active sites $Z^-[OFeOFe]^{2+}Z^-$, $Z^-[FeOFeO]^{2+}Z^-$, and $Z^-[FeOFe]^{2+}Z^-$ unless the H_2O partial pressure becomes $>10^{-7}$ bar. Under these conditions, the inactive site $Z^-[HOFeOFeOH]^{2+}Z^-$ is dominant. At 600 K, significant concentrations of active sites are present only at water partial pressure $<10^{-8}$ bar. Comparing the distribution of species for mononuclear and dinuclear iron sites reveals similar patterns. The fraction of the inactive species is always lower for the dinuclear site, because desorption of water is slightly less endothermic than for mononuclear sites.

In analogy to mononuclear iron sites [37], an Arrhenius plot of the apparent first-order rate coefficient for N_2O decomposition will not be linear and will depend on the H_2O partial pressure in the feed up to a temperature of 725 K (Fig. 3a). In heterogeneous catalysis, a decreased slope of the Arrhenius plot is usually assigned to the transition from the kinetically controlled to the diffusion-controlled regime [45]; however, in the present case, it is the change in the surface composition and the resulting increase in N_2O decomposition activity that cause the nonlinearity of the Arrhenius plot. Fig. 3b shows the change in the most abundant surface species associated with the upper curve of Fig. 3a (10^{-9} bar water pressure). In the temperature regime in which the slope of the Arrhenius plot decreases, the fraction of inactive sites $Z^-[HOFeOFeOH]^{2+}Z^-$ decreases rapidly in favor of the active sites. The activation energy for N_2O dissociation is considerably lower on these sites.

Experimental measurements of the apparent activation energy and pre-exponential factor for N_2O decomposition are most often made over the temperature range of 500–700 K, where small amounts of water have a strong effect on the apparent rate parameters. Heyden et al. [37] have shown that the reported values of the apparent pre-exponential factor correlate with the apparent activation energy over a wide range of values. Virtually all of this variation is attributable to the effects of small concentrations of water vapor in the feed.

The solid lines shown in Fig. 4 represent values of the apparent pre-exponential factor and the apparent activation energies predicted on the basis of the reaction mechanism presented for mononuclear iron sites [33] and the mechanism presented for dinuclear oxygen-bridged iron sites [35]. The latter calculations

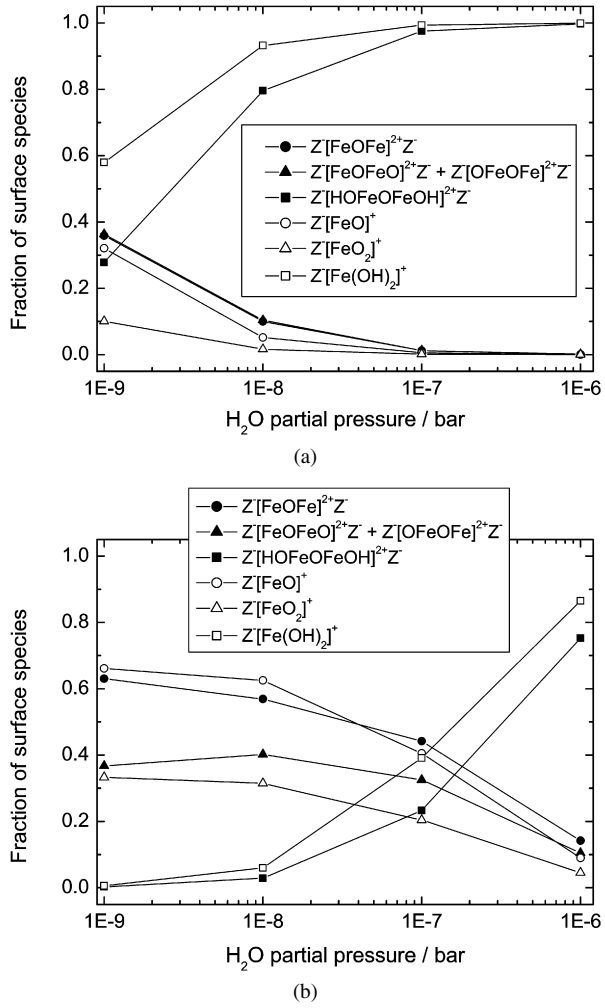

Fig. 2. Surface composition of dinuclear and mononuclear iron sites as a function of H_2O partial pressure at a temperature of (a) 600 K and (b) 700 K.

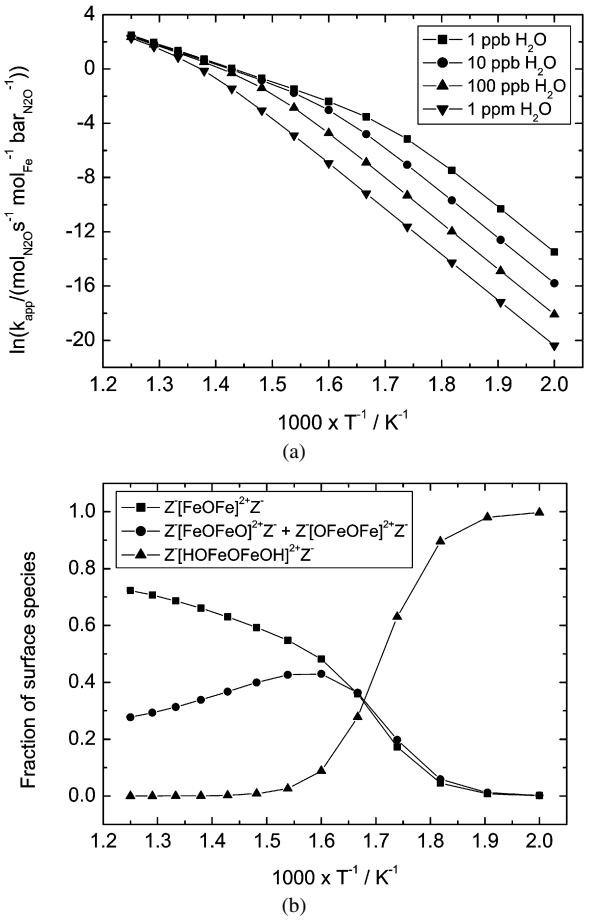

Fig. 3. (a) Arrhenius plots of the first-order N_2O decomposition for different H_2O partial pressures. (b) Variation of catalyst surface with temperature at an H_2O partial pressure of 10^{-9} bar.

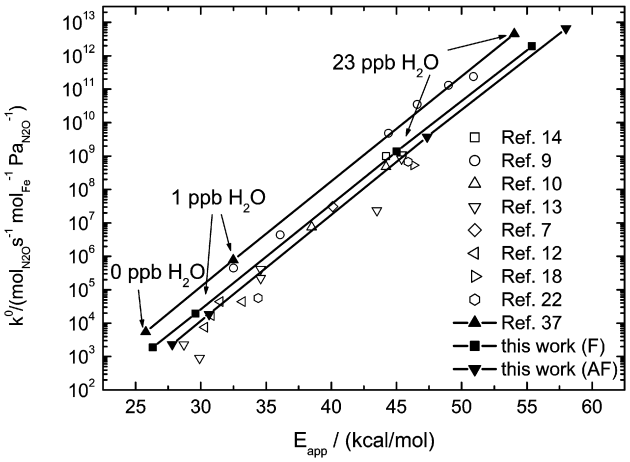

Fig. 4. Plot of logarithm of experimental and computed apparent pre-exponential factor versus apparent activation energy. Open symbols represent experimental data, closed symbols represent simulations from Heyden et al. [37] and the present work for ferromagnetically (F) and antiferromagnetically (AF) coupled iron atoms.

were performed for both antiferromagnetically and ferromagnetically coupled iron atoms. All calculations were done for the temperature range of 600–700 K. The lowest pre-exponential factor and activation energy were calculated for a zero partial pressure of water, while the highest values were obtained for a water pressure of 10^{-7} bar. The figure shows that the reaction rate constants calculated for the dinuclear iron site follow the same compensation relation as the ones for the mononuclear iron site. It is noted that for the same temperature and water partial pressure the specific activity of iron is fourfold higher for the mononuclear sites relative to the dinuclear sites, assuming ferromagnetic coupling between the iron atoms in the latter structure. The apparent reaction rate constants calculated under the assumption of antiferromagnetic coupling of iron atoms in the dinuclear structure are smaller than the ones for the ferromagnetically coupled case by a factor of approximately two.

It should be noted, that the pre-exponential factors for the experimental data presented in Fig. 4 were determined assuming that all iron atoms participate in N_2O decomposition. If only a fraction of the total iron is in the form of mononuclear or dinuclear Fe sites (e.g., part of the Fe is in the form of large inactive iron oxide particles), then the experimental pre-exponential factor will be underestimated. This may be one reason for the wide variation in pre-exponential factors at constant activation energies shown in Fig. 4.

3.2. Simulation of temperature-programmed reaction experiments

The activity of Fe-ZSM-5 for N_2O decomposition has often been studied by temperature-programmed reaction (TPR). It should be noted that such experiments will represent steady-state kinetics only if the catalyst reaches a steady state at each temperature during the temperature increase. If this condition is not satisfied, then discrepancies between steady-state experiments and TPR experiments may arise [46]. However, at temperatures above 700 K, it can be assumed that steady state is reached very rapidly. For this reason, the experimental data against which to compare microkinetic simulations must be chosen with care, because these simulations are based on the assumption of steady state for all species at each reaction temperature. Berlier et al. [20] carried out a TPR experiment for N_2O decomposition at temperatures above 700 K using a sample of Fe-ZSM-5 with very low iron content (0.08 wt%, Fe/Al = 0.017), to minimize the presence of dimeric and larger oxide clusters so as to obtain a single-site model catalyst in which isolated Fe cations predominate. Thus, it is reasonable to assume that for this catalyst, all of the iron is present as mononuclear species, all of which are potentially active. Because the temperatures used in the experiments reported by Berlier et al. exceed 700 K, the influence of water on the observed reaction rates is expected to be small. Fig. 5 compares the experimental results of Berlier et al. [20] with simulations carried out assuming that all of the iron atoms in the catalyst are active and the partial pressure of water vapor in the feed stream is 1 ppm. The reactor is assumed to operate in plug flow, and is represented by a series of 20 stirred tank reactors. Because the simulated curve becomes independent of the water partial pressure in the upper half of the temperature range and is only slightly dependent on the water partial pressure in the lower half, the simulation is virtually parameter-free. It is seen that for this case, the assumption that all active sites are in the form of mononuclear cations gives a very good representation of the experimental data. In contrast, Fig. 5 shows that it is not possible to reproduce the experimental results of Berlier et al. [20] using the reaction rates calculated for the dinuclear iron site. As mentioned above, the reaction rates on dinuclear iron sites are calculated to be smaller by a factor of around 4 at fixed temperature and H_2O partial pressure compared with those for mononuclear iron sites. Although it seems that the rates found for the different active site models can be used to interpret experimental results in terms of the most abundant active species, it should be kept in mind that a factor of 4 can be caused by an error in the activation energy of 2 kcal/mol at temperatures above 700 K, which is in the error range of the B3LYP functional for the determination of activation energies [48].

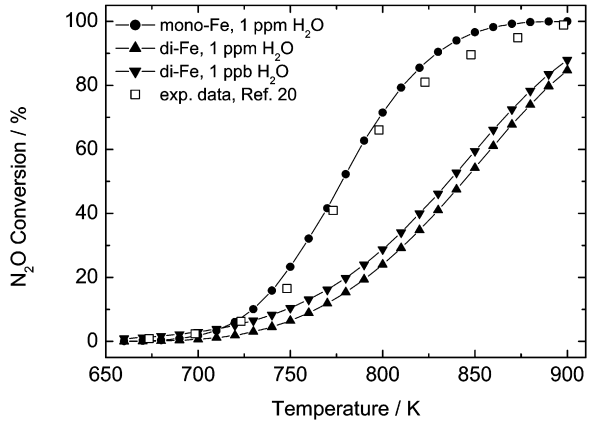

Fig. 5. Experimental and simulated temperature programmed reaction profile for a Fe-ZSM-5 sample with low iron content (0.08 wt%, Fe/Al = 0.017). The experimental results were obtained using 3.3 vol% of N_2O in He (total flow 150 cm^3/min). The simulated TPR profiles were determined for an H_2O partial pressure of 1 ppm for mononuclear iron sites and 1 ppm and 1 ppb for dinuclear iron sites. It is assumed that all iron sites are in the form of mononuclear or dinuclear iron sites, respectively.

A further confirmation of the proposed reaction mechanism on mononuclear iron sites was reported recently by Kondratenko and Pérez-Ramírez [47], who evaluated several kinetic models proposed in the literature for their ability to describe the transient responses of the reactants and products in the temporal analysis of products (TAP) reactor. The best description was obtained considering the reaction scheme proposed by Heyden et al. [33].

For overexchanged Fe-ZSM-5 samples, it is generally accepted that dinuclear or oligonuclear Fe species are present as well as small iron oxide clusters [13,30–32]. However, experiments have shown that small clusters of Fe_2O_3 are not active for N_2O decomposition [10,28]. As shown in Fig. 6a, the reaction mechanism for the dinuclear iron site can be fitted to the experimental results reported by Pirngruber et al. [13] for an overexchanged Fe-ZSM-5 sample prepared by chemical vapor deposition (4 wt% iron content, Fe/Al = 1.1). Good agreement is obtained for a water partial pressure of 10^{-7} bar assuming that 65% of the total iron is present as dinuclear iron sites (i.e., 35% of the total iron is assumed to be in the form of larger inactive iron oxide particles). It should be emphasized that due to water poisoning, only a fraction of these dinuclear iron sites participates in steady-state N_2O decomposition. Fig. 6b shows the fraction of hydroxylated (poisoned) dinuclear iron sites as a function of reaction temperature. At 670 K, approximately 65% of the dinuclear iron sites are hydroxylated (i.e., only 35% participate in N_2O decomposition). As a result, only 23% of the total iron takes part in steady-state N_2O decomposition at this temperature. This fraction of the potentially active iron increases with increasing temperature. Under the same conditions, the mechanism for mononuclear iron sites overpredicts the experimental results by a considerable amount. Although good agreement with the experimental data can be achieved for a simulation based on mononuclear iron sites, such agreement requires the assumption that only 15% of the total iron is in the form of mononuclear iron sites (hydroxylated plus dehydroxylated sites). These results suggest that the iron present in the sample of Fe-ZSM-5 used in those studies most likely contains both mononuclear and dinuclear iron sites.

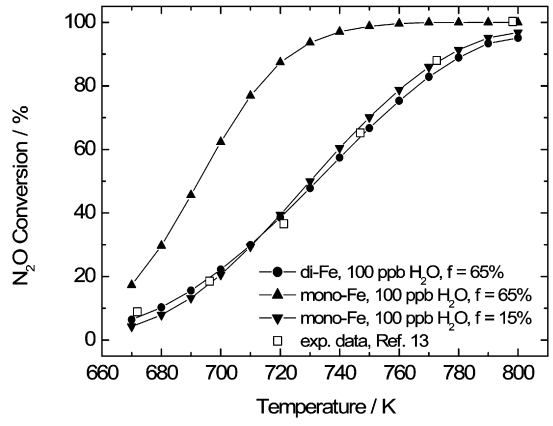

(a)

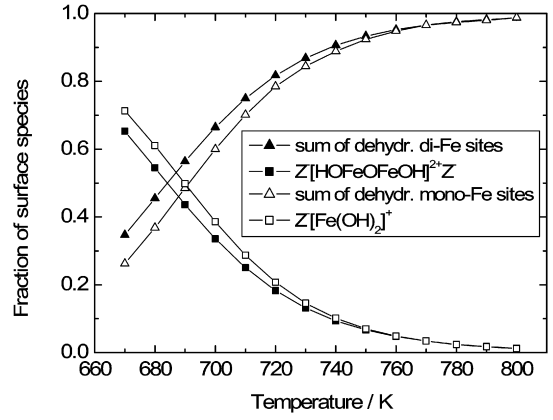

(b)

Fig. 6. (a) Experimental and simulated temperature programmed reaction profile for a Fe-ZSM-5 sample with high iron content (4.0 wt%, Fe/Al = 1.1) prepared by chemical vapor deposition. The experimental results were obtained using 0.25 vol% of N_2O in He (total flow 50 cm^3/min). The simulated TPR profiles were determined for an H_2O partial pressure of 0.1 ppm. Reactor simulations of dinuclear Fe sites have been performed assuming that 65% of the total iron in the system is in the form of dinuclear Fe species (35% of the total iron is in the form of larger inactive iron oxide particles). Reactor simulations of mononuclear Fe sites have been performed assuming that 65 or 15% of the total iron in the system is in the form of mononuclear Fe species (35 or 85% of the total iron is in the form of larger inactive iron oxide particles). (b) Surface composition of dinuclear and mononuclear iron sites in the TPD simulation. The curves for mononuclear iron sites belong to the simulation with $f = 15\%$.

4. Conclusion

Rate parameters for the decomposition of N_2O on dinuclear oxygen bridged iron sites in Fe-ZSM-5 determined from first principles calculations were used to study the influence of water vapor on the distribution of dinuclear iron sites between catalytically active and inactive forms and on the apparent first-order rate constant. The presence of low concentrations of water vapor in the feed stream (ppb to ppm levels) affects the calculated values for the apparent activation energy and pre-exponential factor and thus can explain the wide variation in the experimental values for these quantities, as well as the appearance of an apparent compensation effect. This pattern is very similar to that reported previously for mononuclear iron species in Fe-ZSM-5 [33,37]. Simulations of TPR experiments reported in the literature were carried out based on the mechanism and kinetics developed for mononuclear and dinuclear iron sites. The results obtained for mononuclear sites are in very good agreement with the experimental findings for Fe-ZSM-5 with an iron loading of 0.08 wt% (Fe/Al = 0.017). The simulations suggest that all of the iron in the catalyst is active. Simulations based on mononuclear and dinuclear sites were carried out and compared with experiments conducted with Fe-ZSM-5 containing 4 wt% iron (Fe/Al = 1.1). In this case, good agreement was obtained with the simulations carried out assuming that 65% of the total iron in the catalyst was in the form of dinuclear sites or that 15% of the total iron in the catalyst was in the form of mononuclear sites, and that the content of water vapor in the feed was 100 ppb. The sensitivity of the simulations with respect to the water content was small for both the low-iron-loaded and high-iron-loaded catalysts, because the experiments were all conducted at above >700 K.

Acknowledgments

The authors thank Drs. Jens Döbler, Bernd Kallies, and Uwe Huniar for providing support for use of the TURBOMOLE V5.7 software package. Computations were carried out at the Norddeutscher Verbund für Hoch- und Höchstleistungsrechnen (HLRN) on an IBM p690 Cluster. This work was supported by the Deutsche Forschungsgemeinschaft (priority program SPP 1155), the Fonds der Chemischen Industrie, the Methane Conversion Cooperative (funded by BP), and the Max-Buchner Forschungsstiftung.

Appendix A

All rate parameters computed from DFT calculations are summarized in Tables 1 and 2. Calculated enthalpies of reaction are averaged over the range of 600–800 K. To evaluate whether low spin-inversion probabilities could result in a significant re-

Table 1
Computed rate parameters for elementary steps in nitrous oxide dissociation on ferromagnetically coupled dinuclear oxygen bridged iron sites in Fe-ZSM-5

Reaction	$E^{\dagger a}$, ΔH^b (kcal/mol)	Constant	T (K)		
			600	700	800
1. $Z^-[HOFeOH\_HOFeOH]^{2+}Z^-\{M=11\}$	$\Delta H_1 = 2.5$	K_1, –	2.29E−02	3.08E−02	3.85E−02
$\leftrightarrow Z^-[HOFeOHFe(OH)_2]^{2+}Z^-\{M=11\}$	$E_1{}^{\dagger} = 2.5$	A_1, s^{-1}	1.25E+13	1.46E+13	1.67E+13
		k_1, s^{-1}	1.58E+12	2.48E+12	3.53E+12
	$E_{-1}{}^{\dagger} = 0.0$	A_{-1}, s^{-1}	6.91E+13	8.05E+13	9.18E+13
		k_{-1}, s^{-1}	6.91E+13	8.05E+13	9.18E+13

Table 1 (*continued*)

Reaction	$E^{\dagger}$[a], ΔH[b] (kcal/mol)	Constant	T (K)		
			600	700	800
2. $Z^-[HOFeOHFe(OH)_2]^{2+}Z^-\{M=11\}$	$\Delta H_2 = 2.4$	K_2, –	1.05E−01	1.40E−01	1.73E−01
$\leftrightarrow Z^-[HOFeOFeOH(OH_2)]^{2+}Z^-\{M=11\}$	${E_2}^{\dagger} = 8.1$	A_2, s^{-1}	1.34E+12	1.34E+12	1.33E+12
		k_2, s^{-1}	1.45E+09	3.82E+09	7.93E+09
	${E_{-2}}^{\dagger} = 5.8$	A_{-2}, s^{-1}	1.74E+12	1.72E+12	1.72E+12
		k_{-2}, s^{-1}	1.39E+10	2.73E+10	4.57E+10
3. $Z^-[HOFeOFeOH(OH_2)]^{2+}Z^-\{M=11\}$	$\Delta H_3 = 13.9$	K_3, bar	7.88E+01	4.24E+02	1.45E+03
$\leftrightarrow Z^-[HOFeOFeOH]^{2+}Z^-\{M=11\} + H_2O(g)$	${E_3}^{\dagger} = 14.3$	A_3, s^{-1}	1.25E+13	1.46E+13	1.67E+13
		k_3, s^{-1}	7.40E+07	4.82E+08	2.00E+09
	${E_{-3}}^{\dagger} = 0.0$	A_{-3}, s^{-1} bar^{-1}	9.40E+05	1.14E+06	1.38E+06
		k_{-3} s^{-1} bar^{-1}	9.40E+05	1.14E+06	1.38E+06
4. $Z^-[HOFeOFeOH]^{2+}Z^-\{M=11\} + N_2O(g)$	$\Delta H_4 = -0.8$	K_4, bar^{-1}	5.97E−06	5.33E−06	5.02E−06
$\leftrightarrow Z^-[HOFeOFeOH(ON_2)]^{2+}Z^-\{M=11\}$	${E_4}^{\dagger} = 0.0$	A_4, s^{-1} bar^{-1}	9.51E+06	1.33E+07	1.78E+07
		k_4, s^{-1} bar^{-1}	9.51E+06	1.33E+07	1.78E+07
	${E_{-4}}^{\dagger} = 2.5$	A_{-4}, s^{-1}	1.25E+13	1.46E+13	1.67E+13
		k_{-4}, s^{-1}	1.59E+12	2.49E+12	3.56E+12
5. $Z^-[HOFeOFeOH(ON_2)]^{2+}Z^-\{M=11\}$	$\Delta H_5 = -1.4$	K_5, bar	3.95E+06	3.37E+06	2.93E+06
$\leftrightarrow Z^-[HOFeOOFeOH]^{2+}Z^-\{M=11\} + N_2(g)$	${E_5}^{\dagger} = 40.2$	A_5, s^{-1}	9.73E+11	1.10E+12	1.21E+12
		k_5, s^{-1}	2.19E−03	3.06E−01	1.25E+01
	${E_{-5}}^{\dagger} = 41.3$	A_{-5}, s^{-1} bar^{-1}	6.31E+05	7.30E+05	8.39E+05
		k_{-5}, s^{-1} bar^{-1}	5.53E−10	9.07E−08	4.28E−06
6. $Z^-[HOFeOOFeOH]^{2+}Z^-\{M=11\}$	$\Delta H_6 = 5.2$	K_6, –	4.10E+00	7.61E+00	1.21E+01
$\leftrightarrow Z^-[HOFe\_O_2FeOH]^{2+}Z^-\{M=11\}$	${E_6}^{\dagger} = 6.4$	A_6, s^{-1}	1.14E+13	1.24E+13	1.33E+13
		k_6, s^{-1}	5.15E+10	1.22E+11	2.32E+11
	${E_{-6}}^{\dagger} = 2.1$	A_{-6}, s^{-1}	7.36E+10	7.27E+10	7.22E+10
		k_{-6}, s^{-1}	1.26E+10	1.60E+10	1.92E+10
7. $Z^-[HOFe\_O_2FeOH]^{2+}Z^-\{M=11\}$	$\Delta H_7 = 1.7$	K_7, bar	1.50E+05	1.88E+05	2.15E+05
$\leftrightarrow Z^-[HOFe\_FeOH]^{2+}Z^-\{M=9\} + O_2(g)$	${E_7}^{\dagger} = 9.2$	A_7, s^{-1}	1.04E+14	1.18E+14	1.29E+14
		k_7, s^{-1}	4.81E+10	1.62E+11	4.04E+11
	${E_{-7}}^{\dagger} = 5.8$	A_{-7}, s^{-1} bar^{-1}	4.06E+07	5.48E+07	7.09E+07
		k_{-7}, s^{-1} bar^{-}	3.20E+05	8.64E+05	1.88E+06
8. $Z^-[HOFe\_FeOH]^{2+}Z^-\{M=9\} + N_2O(g)$	$\Delta H_8 = -0.2$	K_8, bar^{-1}	3.97E−06	3.79E−06	3.78E−06
$\leftrightarrow Z^-[HOFe(ON_2)\_FeOH]^{2+}Z^-\{M=9\}$	${E_8}^{\dagger} = 0.0$	A_8, s^{-1} bar^{-1}	6.56E+06	9.76E+06	1.38E+07
		k_8, s^{-1} bar^{-1}	6.56E+06	9.76E+06	1.38E+07
	${E_{-8}}^{\dagger} = 2.4$	A_{-8}, s^{-1}	1.25E+13	1.46E+13	1.67E+13
		k_{-8}, s^{-1}	1.65E+12	2.58E+12	3.66E+12
9. $Z^-[HOFe(ON_2)\_FeOH]^{2+}Z^-\{M=9\}$	$\Delta H_9 = -15.0$	K_9, bar	4.06E+10	6.86E+09	1.76E+09
$\leftrightarrow Z^-[HOFeO\_FeOH]^{2+}Z^-\{M=9\} + N_2(g)$	${E_9}^{\dagger} = 25.9$	A_9, s^{-1}	1.52E+12	1.66E+12	1.80E+12
		k_9, s^{-1}	5.66E+02	1.38E+04	1.53E+05
	${E_{-9}}^{\dagger} = 39.4$	A_{-9}, s^{-1} bar^{-1}	3.31E+06	4.22E+06	5.25E+06
		k_{-9}, s^{-1} bar^{-1}	1.39E−08	2.01E−06	8.66E−05
10. $Z^-[HOFeO\_FeOH]^{2+}Z^-\{M=9\}$	$\Delta H_{10} = -27.9$	K_{10}, –	2.85E+09	9.95E+07	8.09E+06
$\leftrightarrow Z^-[HOFeOFeOH]^{2+}Z^-\{M=11\}$	${E_{10}}^{\dagger} = 0.1$	A_{10}, s^{-1}	2.18E+12	2.39E+12	2.59E+12
		k_{10}, s^{-1}	2.06E+12	2.28E+12	2.48E+12
	${E_{-10}}^{\dagger} = 28.4$	A_{-10}, s^{-1}	1.61E+13	1.70E+13	1.77E+13
		k_{-10}, s^{-1}	7.22E+02	2.29E+04	3.07E+05
11. $Z^-[HOFeO\_FeOH]^{2+}Z^-\{M=9\} + N_2O(g)$	$\Delta H_{11} = 0.2$	K_{11}, bar^{-1}	5.31E−06	5.35E−06	5.54E−06
$\leftrightarrow Z^-[HOFeO\_(N_2O)FeOH]^{2+}Z^-\{M=9\}$	${E_{11}}^{\dagger} = 0.0$	A_{11}, s^{-1} bar^{-1}	1.56E+07	2.25E+07	3.11E+07
		k_{11}, s^{-1} bar^{-1}	1.56E+07	2.25E+07	3.11E+07
	${E_{-11}}^{\dagger} = 1.7$	A_{-11}, s^{-1}	1.25E+13	1.46E+13	1.67E+13
		k_{-11}, s^{-1}	2.93E+12	4.21E+12	5.62E+12
12. $Z^-[HOFeO\_(N_2O)FeOH]^{2+}Z^-\{M=9\}$	$\Delta H_{12} = -11.9$	K_{12}, bar	9.38E+08	2.28E+08	7.70E+07
$\leftrightarrow Z^-[HOFeO\_OFeOH]^{2+}Z^-\{M=9\} + N_2(g)$	${E_{12}}^{\dagger} = 25.0$	A_{12}, s^{-1}	6.55E+12	7.45E+12	8.29E+12
		k_{12}, s^{-1}	5.12E+03	1.17E+05	1.23E+06
	${E_{-12}}^{\dagger} = 35.5$	A_{-12}, s^{-1} bar^{-1}	4.87E+07	6.45E+07	8.22E+07

(*continued on next page*)

Table 1 (*continued*)

Reaction	$E^{\dagger}$[a], ΔH[b] (kcal/mol)	Constant	T (K)		
			600	700	800
		k_{-12}, s^{-1} bar^{-1}	5.46E−06	5.11E−04	1.59E−02
13. $Z^-[HOFeO\_OFeOH]^{2+}Z^-\{M=9\}$	$\Delta H_{13} = -18.5$	K_{13}, –	1.35E+07	1.46E+06	2.79E+05
$\leftrightarrow Z^-[HOFeOOFeOH]^{2+}Z^-\{M=11\}$	$E_{13}{}^{\dagger} = 9.4$	A_{13}, s^{-1}	7.72E+12	9.15E+12	1.05E+13
		k_{13}	3.01E+09	1.09E+10	2.91E+10
	$E_{-13}{}^{\dagger} = 29.0$	A_{-13}, s^{-1}	8.13E+12	8.46E+12	8.72E+12
		k_{-13}, s^{-1}	2.23E+02	7.48E+03	1.04E+05
14. $Z^-[HOFe\_FeOH]^{2+}Z^-\{M=9\}$	$\Delta H_{14} = -10.9$	K_{14}, –	4.20E+02	1.13E+02	4.25E+01
$\leftrightarrow Z^-[FeOHFeOH]^{2+}Z^-\{M=9\}$	$E_{14}{}^{\dagger} = 1.9$	A_{14}, s^{-1}	2.46E+11	2.06E+11	1.78E+11
		k_{14}, s^{-1}	4.85E+10	5.13E+10	5.27E+10
	$E_{-14}{}^{\dagger} = 12.7$	A_{-14}, s^{-1}	5.09E+12	4.33E+12	3.77E+12
		k_{-14}, s^{-1}	1.15E+08	4.53E+08	1.24E+09
15. $Z^-[FeOHFeOH]^{2+}Z^-\{M=9\} + N_2O(g)$	$\Delta H_{15} = -2.2$	K_{15}, bar^{-1}	7.07E−05	5.33E−05	4.43E−05
$\leftrightarrow Z^-[(N_2O)FeOHFeOH]^{2+}Z^-\{M=9\}$	$E_{15}{}^{\dagger} = 0.0$	A_{15}, s^{-1} bar^{-1}	2.99E+07	4.26E+07	5.82E+07
		k_{15}, s^{-1} bar^{-1}	2.99E+07	4.26E+07	5.82E+07
	$E_{-15}{}^{\dagger} = 4.0$	A_{-15}, s^{-1}	1.25E+13	1.46E+13	1.67E+13
		k_{-15}, s^{-1}	4.23E+11	8.01E+11	1.32E+12
16. $Z^-[(N_2O)FeOHFeOH]^{2+}Z^-\{M=9\}$	$\Delta H_{16} = -8.4$	K_{16}, bar	7.05E+07	2.61E+07	1.21E+07
$\leftrightarrow Z^-[OFeOHFeOH]^{2+}Z^-\{M=9\} + N_2(g)$	$E_{16}{}^{\dagger} = 32.3$	A_{16}, s^{-1}	2.25E+12	2.29E+12	2.30E+12
		k_{16}, s^{-1}	3.74E+00	1.83E+02	3.37E+03
	$E_{-16}{}^{\dagger} = 39.7$	A_{-16}, s^{-1} bar^{-1}	1.58E+07	1.79E+07	1.99E+07
		k_{-16}, s^{-1} bar^{-1}	5.30E−08	7.01E−06	2.77E−04
17. $Z^-[OFeOHFeOH]^{2+}Z^-\{M=11\}$	$\Delta H_{17} = 3.6$	K_{17}, –	5.60E−03	8.67E−03	1.20E−02
$\leftrightarrow Z^-[OFeOHFeOH]^{2+}Z^-\{M=9\}$	$E_{17}{}^{\dagger} = 5.6$	A_{17}, s^{-1}	1.25E+13	1.46E+13	1.67E+13
		k_{17}, s^{-}	1.18E+11	2.68E+11	5.04E+11
	$E_{-17}{}^{\dagger} = 1.6$	A_{-17}, s^{-1}	7.73E+13	9.42E+13	1.11E+14
		k_{-17}, s^{-1}	2.10E+13	3.09E+13	4.19E+13
18. $Z^-[HOFeOFeOH]^{2+}Z^-\{M=11\}$	$\Delta H_{18} = 18.0$	K_{18}, –	8.14E−07	7.03E−06	3.53E−05
$\leftrightarrow Z^-[OFeOHFeOH]^{2+}Z^-\{M=11\}$	$E_{18}{}^{\dagger} = 24.3$	A_{18}, s^{-1}	3.76E+12	3.76E+12	3.76E+12
		k_{18}, s^{-1}	5.39E+03	9.87E+04	8.76E+05
	$E_{-18}{}^{\dagger} = 6.2$	A_{-18}, s^{-1}	1.20E+12	1.21E+12	1.23E+12
		k_{-18}, s^{-1}	6.62E+09	1.40E+10	2.48E+10
19. $Z^-[HOFeOHFeO]^{2+}Z^-\{M=11\}$	$\Delta H_{19} = 2.8$	K_{19}, –	4.70E−03	6.84E−03	9.03E−03
$\leftrightarrow Z^-[HOFeOHFeO]^{2+}Z^{-1}\{M=9\}$[c]	$E_{19}{}^{\dagger} = 5.4$	A_{19}, s^{-1}	1.25E+13	1.46E+13	1.67E+13
		k_{19}, s^{-1}	1.36E+11	3.04E+11	5.63E+11
	$E_{-19}{}^{\dagger} = 1.8$	A_{-19}, s^{-1}	1.32E+14	1.62E+14	1.94E+14
		k_{-19}, s^{-1}	2.90E+13	4.44E+13	6.23E+13
20. $Z^-[HOFeOFeOH]^{2+}Z^-\{M=11\}$	$\Delta H_{20} = 17.1$	K_{20}, –	1.07E−06	8.61E−06	4.10E−05
$\leftrightarrow Z^-[HOFeOHFeO]^{2+}Z^-\{M=11\}$[c]	$E_{20}{}^{\dagger} = 23.9$	A_{20}, s^{-1}	6.56E+11	5.66E+11	4.98E+11
		k_{20}, s^{-1}	1.32E+03	1.98E+04	1.49E+05
	$E_{-20}{}^{\dagger} = 6.3$	A_{-20}, s^{-1}	2.38E+11	2.10E+11	1.89E+11
		k_{-20}, s^{-1}	1.23E+09	2.30E+09	3.64E+09
21. $Z^-[OFeOHFeOH]^{2+}Z^-\{M=11\} + N_2O(g)$	$\Delta H_{21} = 0.0$	K_{21}, bar^{-1}	2.28E−05	2.25E−05	2.29E−05
$\leftrightarrow Z^-[(N_2O)OFeOHFeOH]^{2+}Z^-\{M=11\}$	$E_{21}{}^{\dagger} = 0.0$	A_{21}, s^{-1} bar^{-1}	7.41E+07	1.03E+08	1.39E+08
		k_{21}, s^{-1} bar^{-1}	7.41E+07	1.03E+08	1.39E+08
	$E_{-21}{}^{\dagger} = 1.6$	A_{-21}, s^{-1}	1.25E+13	1.46E+13	1.67E+13
		k_{-21}, s^{-1}	3.25E+12	4.60E+12	6.07E+12
22. $Z^-[(N_2O)OFeOHFeOH]^{2+}Z^-\{M=11\}$	$\Delta H_{22} = -6.8$	K_{22}, bar	1.12E+07	5.02E+06	2.70E+06
$\leftrightarrow Z^-[OOFeOHFeOH]^{2+}Z^-\{M=11\} + N_2(g)$	$E_{22}{}^{\dagger} = 34.7$	A_{22}, s^{-1}	2.73E+11	3.00E+11	3.24E+11
		k_{22}, s^{-1}	6.39E−02	4.46E+00	1.09E+02
	$E_{-22}{}^{\dagger} = 40.9$	A_{-22}, s^{-1} bar^{-1}	4.53E+06	5.25E+06	6.03E+06
		k_{-22}, s^{-1} bar^{-1}	5.72E−09	8.90E−07	4.03E−05
23. $Z^-[OOFeOHFeOH]^{2+}Z^-\{M=11\}$	$\Delta H_{23} = -15.0$	K_{23}, –	3.30E+06	5.45E+05	1.41E+05
$\leftrightarrow Z^-[O_2FeOHFeOH]^{2+}Z^-\{M=11\}$	$E_{23}{}^{\dagger} = 11.1$	A_{23}, s^{-1}	1.11E+13	1.18E+13	1.23E+13
		k_{23}, s^{-1}	9.83E+08	3.95E+09	1.12E+10

Table 1 (*continued*)

Reaction	$E^{\dagger}$[a], ΔH[b] (kcal/mol)	Constant	T (K)		
			600	700	800
	$E_{-23}{}^{\dagger} = 26.5$	A_{-23}, s^{-1}	1.40E+12	1.41E+12	1.42E+12
		k_{-23}, s^{-1}	2.98E+02	7.24E+03	7.94E+04
24. $Z^-[O_2FeOHFeOH]^{2+}Z^-\{M=11\}$	$\Delta H_{24} = -2.5$	K_{24}, bar	8.93E+06	6.72E+06	5.28E+06
$\leftrightarrow Z^-[FeOHFeOH]^{2+}Z^-\{M=9\} + O_2(g)$	$E_{24}{}^{\dagger} = 0.2$	A_{24}, s^{-1}	1.52E+09	6.25E+09	1.80E+10
		k_{24}, s^{-1}	1.31E+09	5.48E+09	1.61E+10
	$E_{-24}{}^{\dagger} = 1.7$	A_{-24}, s^{-1} bar^{-1}	6.00E+02	2.74E+03	8.78E+03
		k_{-24}, s^{-1} bar^{-1}	1.46E+02	8.16E+02	3.05E+03
25. $Z^-[OFeOHFeOH]^{2+}Z^-\{M=9\}$	$\Delta H_{25} = 3.9$	K_{25}, –	2.27E−01	3.64E−01	5.17E−01
$\leftrightarrow Z^-[OFeOFeOH_2]^{2+}Z^-\{M=9\}$	$E_{25}{}^{\dagger} = 7.9$	A_{25}, s^{-1}	1.74E+12	1.50E+12	1.32E+12
		k_{25}, s^{-1}	2.38E+09	5.28E+09	9.41E+09
	$E_{-25}{}^{\dagger} = 4.0$	A_{-25}, s^{-1}	3.07E+11	2.62E+11	2.29E+11
		k_{-25}, s^{-1}	1.05E+10	1.45E+10	1.82E+10
26. $Z^-[OFeOFeOH_2]^{2+}Z^-\{M=9\}$	$\Delta H_{26} = 16.5$	K_{26}, bar	8.48E−02	6.28E−01	2.74E+00
$\leftrightarrow Z^-[OFeOFe]^{2+}Z^-\{M=9\} + H_2O(g)$	$E_{26}{}^{\dagger} = 17.7$	A_{26}, s^{-1}	1.25E+13	1.46E+13	1.67E+13
		k_{26}, s^{-1}	4.48E+06	4.36E+07	2.44E+08
	$E_{-26}{}^{\dagger} = 0.0$	A_{-26}, s^{-1} bar^{-1}	5.29E+07	6.94E+07	8.93E+07
		k_{-26}, s^{-1} bar^{-1}	5.29E+07	6.94E+07	8.93E+07
27. $Z^-[HOFeOHFeO]^{2+}Z^-\{M=9\}$	$\Delta H_{27} = 7.7$	K_{27}, –	1.79E−01	3.19E−01	4.88E−01
$\leftrightarrow Z^-[H_2OFeOFeO]^{2+}Z^-\{M=9\}$[c]	$E_{27}{}^{\dagger} = 10.7$	A_{27}, s^{-1}	5.12E+12	5.07E+12	5.04E+12
		k_{27}, s^{-1}	6.28E+08	2.25E+09	5.87E+09
	$E_{-27}{}^{\dagger} = 6.1$	A_{-27}, s^{-1}	5.68E+11	5.54E+11	5.47E+11
		k_{-27}, s^{-1}	3.50E+09	7.07E+09	1.20E+10
28. $Z^-[H_2OFeOFeO]^{2+}Z^-\{M=9\}$	$\Delta H_{28} = 16.9$	K_{28}, bar	1.36E+00	6.81E+00	2.21E+01
$\leftrightarrow Z^-[FeOFeO]^{2+}Z^-\{M=9\} + H_2O(g)$[c]	$E_{28}{}^{\dagger} = 14.3$	A_{28}, s^{-1}	1.25E+13	1.46E+13	1.67E+13
		k_{28}, s^{-1}	7.58E+07	4.92E+08	2.04E+09
	$E_{-28}{}^{\dagger} = 0.0$	A_{-28}, s^{-1} bar^{-1}	5.57E+07	7.22E+07	9.22E+07
		k_{-28}, s^{-1} bar^{-1}	5.57E+07	7.22E+07	9.22E+07
29. $Z^-[FeOHFeOH]^{2+}Z^-\{M=9\}$	$\Delta H_{29} = 8.8$	K_{29}, –	1.17E−02	3.37E−02	7.43E−02
$\leftrightarrow Z^-[FeOFeOH_2]^{2+}Z^-\{M=9\}$	$E_{29}{}^{\dagger} = 13.7$	A_{29}, s^{-1}	2.79E+12	2.68E+12	2.60E+12
		k_{29}, s^{-1}	2.89E+07	1.43E+08	4.74E+08
	$E_{-29}{}^{\dagger} = 4.7$	A_{-29}, s^{-1}	1.29E+11	1.26E+11	1.24E+11
		k_{-29}, s^{-1}	2.48E+09	4.24E+09	6.38E+09
30. $Z^-[FeOFeOH_2]^{2+}Z^-\{M=9\}$	$\Delta H_{30} = 12.8$	K_{30}, bar	7.97E−01	3.76E+00	1.17E+01
$\leftrightarrow Z^-[FeOFe]^{2+}Z^-\{M=9\} + H_2O(g)$	$E_{30}{}^{\dagger} = 13.9$	A_{30}, s^{-1}	1.25E+13	1.46E+13	1.67E+13
		k_{30}, s^{-1}	1.11E+08	6.84E+08	2.72E+09
	$E_{-30}{}^{\dagger} = 0.0$	A_{-30}, s^{-1} bar^{-1}	1.40E+08	1.82E+08	2.33E+08
		k_{-30}, s^{-1} bar^{-1}	1.40E+08	1.82E+08	2.33E+08
31. $Z^-[FeOFe]^{2+}Z^-\{M=9\} + N_2O(g)$	$\Delta H_{31} = -2.6$	K_{31}, bar^{-1}	5.46E−05	3.93E−05	3.16E−05
$\leftrightarrow Z^-[(N_2O)FeOFe]^{2+}Z^-\{M=9\}$	$E_{31}{}^{\dagger} = 0.0$	A_{31}, s^{-1} bar^{-1}	1.79E+07	2.53E+07	3.44E+07
		k_{31}, s^{-1} bar^{-1}	1.79E+07	2.53E+07	3.44E+07
	$E_{-31}{}^{\dagger} = 4.3$	A_{-31}, s^{-1}	1.25E+13	1.46E+13	1.67E+13
		k_{-31}, s^{-1}	3.28E+11	6.44E+11	1.09E+12
32. $Z^-[(N_2O)FeOFe]^{2+}Z^-\{M=9\}$	$\Delta H_{32} = -9.0$	K_{32}, bar	1.89E+08	6.38E+07	2.77E+07
$\leftrightarrow Z^-[OFeOFe]^{2+}Z^-\{M=9\} + N_2(g)$	$E_{32}{}^{\dagger} = 27.5$	A_{32}, s^{-1}	9.83E+12	1.13E+13	1.27E+13
		k_{32}, s^{-1}	9.07E+02	2.83E+04	3.77E+05
	$E_{-32}{}^{\dagger} = 35.9$	A_{-32}, s^{-1} bar^{-1}	6.01E+07	7.47E+07	9.06E+07
		k_{-32}, s^{-1} bar^{-1}	4.79E−06	4.43E−04	1.36E−02
33. $Z^-[OFeOFe]^{2+}Z^-\{M=9\} + N_2O(g)$	$\Delta H_{33} = -3.0$	K_{33}, bar^{-1}	7.06E−05	4.82E−05	3.72E−05
$\leftrightarrow Z^-[OFeOFe(ON_2)]^{2+}Z^-\{M=9\}$	$E_{33}{}^{\dagger} = 0.0$	A_{33}, s^{-1} bar^{-1}	1.64E+07	2.31E+07	3.12E+07
		k_{33}, s^{-1} bar^{-1}	1.64E+07	2.31E+07	3.12E+07
	$E_{-33}{}^{\dagger} = 4.7$	A_{-33}, s^{-1}	1.25E+13	1.46E+13	1.67E+13
		k_{-33}, s^{-1}	2.33E+11	4.80E+11	8.40E+11
34. $Z^-[OFeOFe(ON_2)]^{2+}Z^-\{M=9\}$	$\Delta H_{34} = -9.6$	K_{34}, bar	1.04E+08	3.35E+07	1.40E+07
$\leftrightarrow Z^-[OFeOFeO]^{2+}Z^-\{M=9\} + N_2(g)$	$E_{34}{}^{\dagger} = 27.7$	A_{34}, s^{-1}	8.53E+13	9.89E+13	1.12E+14

(*continued on next page*)

Table 1 (*continued*)

Reaction	$E^{\dagger}$[a], ΔH[b] (kcal/mol)	Constant	T (K)		
			600	700	800
		k_{34}, s^{-1}	6.93E+03	2.22E+05	3.02E+06
	$E_{-34}{}^{\dagger} = 36.3$	A_{-34}, s^{-1} bar^{-1}	1.10E+09	1.41E+09	1.76E+09
		k_{-34}, s^{-1} bar^{-1}	6.66E−05	6.63E−03	2.15E−01
35. $Z^-[FeOFe]^{2+}Z^-\{M=9\} + N_2O(g)$	$\Delta H_{35} = -2.7$	K_{35}, bar^{-1}	9.38E−05	6.63E−05	5.25E−05
$\leftrightarrow Z^-[FeOFe(ON_2)]^{2+}Z^-\{M=9\}$	$E_{35}{}^{\dagger} = 0.0$	A_{35}, s^{-1} bar^{-1}	2.63E+07	3.73E+07	5.07E+07
		k_{35}, s^{-1} bar^{-1}	2.63E+07	3.73E+07	5.07E+07
	$E_{-35}{}^{\dagger} = 4.5$	A_{-35}, s^{-1}	1.25E+13	1.46E+13	1.67E+13
		k_{-35}, s^{-1}	2.80E+11	5.62E+11	9.65E+11
36. $Z^-[FeOFe(ON_2)]^{2+}Z^-\{M=9\}$	$\Delta H_{36} = -12.6$	K_{36}, bar	1.55E+09	3.47E+08	1.11E+08
$\leftrightarrow Z^-[FeOFeO]^{2+}Z^-\{M=9\} + N_2(g)$	$E_{36}{}^{\dagger} = 25.6$	A_{36}, s^{-1}	7.09E+11	7.93E+11	8.71E+11
		k_{36}, s^{-1}	3.45E+02	8.26E+03	9.03E+04
	$E_{-36}{}^{\dagger} = 37.2$	A_{-36}, s^{-1} bar^{-1}	8.04E+06	9.91E+06	1.20E+07
		k_{-36}, s^{-1} bar^{-1}	2.23E−07	2.38E−05	8.14E−04
37. $Z^-[FeOFeO]^{2+}Z^-\{M=9\} + N_2O(g)$	$\Delta H_{37} = -3.6$	K_{37}, bar^{-1}	1.01E−04	6.44E−05	4.72E−05
$\leftrightarrow Z^-[(N_2O)FeOFeO]^{2+}Z^-\{M=9\}$	$E_{37}{}^{\dagger} = 0.0$	A_{37}, s^{-1} bar^{-1}	1.42E+07	2.00E+07	2.71E+07
		k_{37}, s^{-1} bar^{-1}	1.42E+07	2.00E+07	2.71E+07
	$E_{-37}{}^{\dagger} = 5.3$	A_{-37}, s^{-1}	1.25E+13	1.46E+13	1.67E+13
		k_{-37}, s^{-1}	1.40E+11	3.11E+11	5.75E+11
38. $Z^-[(N_2O)FeOFeO]^{2+}Z^-\{M=9\}$	$\Delta H_{38} = -5.4$	K_{38}, bar	5.17E+06	2.73E+06	1.66E+06
$\leftrightarrow Z^-[OFeOFeO]^{2+}Z^-\{M=9\} + N_2(g)$	$E_{38}{}^{\dagger} = 30.1$	A_{38}, s^{-1}	5.05E+13	5.89E+13	6.66E+13
		k_{38}, s^{-1}	5.26E+02	2.27E+04	3.86E+05
	$E_{-38}{}^{\dagger} = 34.7$	A_{-38}, s^{-1} bar^{-1}	4.43E+08	5.66E+08	7.01E+08
		k_{-38}, s^{-1} bar^{-1}	1.02E−04	8.30E−03	2.32E−01
39. $Z^-[OFeOFeO]^{2+}Z^-\{M=9\}$	$\Delta H_{39} = 8.3$	K_{39}, –	1.91E−01	5.18E−01	1.10E+00
$\leftrightarrow Z^-[FeOOFeO]^{2+}Z^-\{M=9\}$	$E_{39}{}^{\dagger} = 27.3$	A_{39}, s^{-1}	3.26E+14	3.90E+14	4.48E+14
		k_{39}, s^{-1}	3.79E+04	1.19E+06	1.58E+07
	$E_{-39}{}^{\dagger} = 20.0$	A_{-39}, s^{-1}	3.98E+12	4.17E+12	4.33E+12
		k_{-39}, s^{-1}	1.98E+05	2.30E+06	1.44E+07
40. $Z^-[FeOOFeO]^{2+}Z^-\{M=9\}$	$\Delta H_{40} = -5.3$	K_{40}, –	4.74E+00	2.51E+00	1.55E+00
$\leftrightarrow Z^-[FeO_2FeO]^{2+}Z^-\{M=9\}$	$E_{40}{}^{\dagger} = 6.2$	A_{40}, s^{-1}	9.36E+12	9.88E+12	1.03E+13
		k_{40}, s^{-1}	5.05E+10	1.12E+11	2.05E+11
	$E_{-40}{}^{\dagger} = 11.0$	A_{-40}, s^{-1}	1.08E+14	1.22E+14	1.33E+14
		k_{-40}, s^{-1}	1.07E+10	4.49E+10	1.32E+11
41. $Z^-[FeO_2FeO]^{2+}Z^-\{M=9\}$	$\Delta H_{41} = -19.4$	K_{41}, –	1.10E+08	1.06E+07	1.85E+06
$\leftrightarrow Z^-[FeOFeO_2]^{2+}Z^-\{M=9\}$	$E_{41}{}^{\dagger} = 25.3$	A_{41}, s^{-1}	1.07E+13	1.20E+13	1.32E+13
		k_{41}, s^{-1}	6.48E+03	1.51E+05	1.61E+06
	$E_{-41}{}^{\dagger} = 45.2$	A_{-41}, s^{-1}	1.72E+12	1.84E+12	1.94E+12
		k_{-41}, s^{-1}	5.92E−05	1.42E−02	8.70E−01
42. $Z^-[FeOFeO_2]^{2+}Z^-\{M=9\}$	$\Delta H_{42} = -4.8$	K_{42}, –	1.06E+02	5.95E+01	3.86E+01
$\leftrightarrow Z^-[FeOFeO_2]^{2+}Z^-\{M=11\}$	$E_{42}{}^{\dagger} = 7.6$	A_{42}, s^{-1}	1.25E+13	1.46E+13	1.67E+13
		k_{42}, s^{-1}	2.21E+10	6.36E+10	1.43E+11
	$E_{-42}{}^{\dagger} = 12.3$	A_{-42}, s^{-1}	6.25E+12	7.36E+12	8.47E+12
		k_{-42}, s^{-1}	2.08E+08	1.07E+09	3.72E+09
43. $Z^-[FeOFeO_2]^{2+}Z^-\{M=11\}$	$\Delta H_{43} = 7.1$	K_{43}, bar	8.41E+03	2.00E+04	3.72E+04
$\leftrightarrow Z^-[FeOFe]^{2+}Z^-\{M=9\} + O_2(g)$	$E_{43}{}^{\dagger} = 8.1$	A_{43}, s^{-1}	7.78E+13	8.46E+13	9.00E+13
		k_{43}, s^{-1}	9.00E+10	2.57E+11	5.64E+11
	$E_{-43}{}^{\dagger} = 0.02$	A_{-43}, s^{-1} bar^{-1}	1.08E+07	1.30E+07	1.53E+07
		k_{-43}, s^{-1} bar^{-1}	1.07E+07	1.28E+07	1.52E+07

[a] Calculated activation energy including zero-point energy correction.
[b] Calculated enthalpy averaged over 600–800 K.
[c] Reaction has not been described in Ref. [35].

duction of the rates of spin-surface crossing, thermally averaged Landau–Zener transition probabilities were calculated; these are summarized in Table 3 for spin–orbit coupling energies of 395 and 825 J/mol at several temperatures. All spin-inversion transmission coefficients were >0.03 at 700 K. As a result, failure to correct reaction rates for spin-inversion probabilities <1

Table 2
Computed rate parameters for elementary steps in nitrous oxide dissociation on antiferromagnetically coupled dinuclear oxygen bridged iron sites in Fe-ZSM-5

Reaction[a]	$E^{\dagger}$[b], ΔH[c] (kcal/mol)	Constant	T (K)		
			600	700	800
1. $Z^-[HOFeOFeOH]^{2+}Z^-\{M=1\} \leftrightarrow Z^-[OFeOFe]^{2+}Z^-\{M=1\} + H_2O(g)$[d]	$\Delta H_1 = 46.7$	K_1, bar	3.74E−12	1.04E−09	6.84E−08
	$E_1{}^{\dagger} = 48.1$	A_1, s^{-1}	1.25E+13	1.46E+13	1.67E+13
		k_1, s^{-1}	3.74E−05	1.39E−02	1.20E+00
	$E_{-1}{}^{\dagger} = 0.0$	A_{-1}, s^{-1} bar^{-1}	1.00E+07	1.33E+07	1.75E+07
		k_{-1}, s^{-1} bar^{-1}	1.00E+07	1.33E+07	1.75E+07
2. $Z^-[HOFeOFeOH]^{2+}Z^-\{M=1\} \leftrightarrow Z^-[FeOFeO]^{2+}Z^-\{M=1\} + H_2O(g)$[d]	$\Delta H_2 = 43.2$	K_2, bar	6.89E−11	1.27E−08	6.08E−07
	$E_2{}^{\dagger} = 44.7$	A_2, s^{-1}	1.25E+13	1.46E+13	1.67E+13
		k_2, s^{-1}	6.53E−04	1.61E−01	1.02E+01
	$E_{-2}{}^{\dagger} = 0.0$	A_{-2}, s^{-1} bar^{-1}	9.48E+06	1.27E+07	1.68E+07
		k_{-2}, s^{-1} bar^{-1}	9.48E+06	1.27E+07	1.68E+07
3. (31.) $Z^-[FeOFe]^{2+}Z^-\{M=1\} + N_2O(g) \leftrightarrow Z^-[(N_2O)FeOFe]^{2+}Z^-\{M=1\}$	$\Delta H_3 = -2.3$	K_3, bar^{-1}	3.27E−05	2.43E−05	1.99E−05
	$E_3{}^{\dagger} = 0.0$	A_3, s^{-1} bar^{-1}	1.37E+07	1.93E+07	2.60E+07
		k_3, s^{-1} bar^{-1}	1.37E+07	1.93E+07	2.60E+07
	$E_{-3}{}^{\dagger} = 4.0$	A_{-3}, s^{-1}	1.25E+13	1.46E+13	1.67E+13
		k_{-3}, s^{-1}	4.19E+11	7.94E+11	1.31E+12
4. (32.) $Z^-[(N_2O)FeOFe]^{2+}Z^-\{M=1\} \leftrightarrow Z^-[OFeOFe]^{2+}Z^-\{M=1\} + N_2(g)$	$\Delta H_4 = -8.2$	K_4, bar	7.99E+07	3.05E+07	1.45E+07
	$E_4{}^{\dagger} = 26.1$	A_4, s^{-1}	1.03E+13	1.18E+13	1.32E+13
		k_4, s^{-1}	3.30E+03	8.58E+04	9.98E+05
	$E_{-4}{}^{\dagger} = 33.4$	A_{-4}, s^{-1} bar^{-1}	6.20E+07	7.71E+07	9.35E+07
		k_{-4}, s^{-1} bar^{-1}	4.12E−05	2.81E−03	6.88E−02
5. (33.) $Z^-[OFeOFe]^{2+}Z^-\{M=1\} + N_2O(g) \leftrightarrow Z^-[OFeOFe(ON_2)]^{2+}Z^-\{M=1\}$	$\Delta H_5 = -3.0$	K_5, bar^{-1}	6.64E−05	4.54E−05	3.50E−05
	$E_5{}^{\dagger} = 0.0$	A_5, s^{-1} bar^{-1}	1.56E+07	2.20E+07	2.97E+07
		k_5, s^{-1} bar^{-1}	1.56E+07	2.20E+07	2.97E+07
	$E_{-5}{}^{\dagger} = 4.7$	A_{-5}, s^{-1}	1.25E+13	1.46E+13	1.67E+13
		k_{-5}, s^{-1}	2.36E+11	4.85E+11	8.48E+11
6. (34.) $Z^-[OFeOFe(ON_2)]^{2+}Z^-\{M=1\} \leftrightarrow Z^-[OFeOFeO]^{2+}Z^-\{M=1\} + N_2(g)$	$\Delta H_6 = -8.6$	K_6, bar	3.91E+07	1.41E+07	6.44E+06
	$E_6{}^{\dagger} = 27.4$	A_6, s^{-1}	1.09E+14	1.26E+14	1.41E+14
		k_6, s^{-1}	1.11E+04	3.43E+05	4.53E+06
	$E_{-6}{}^{\dagger} = 35.0$	A_{-6}, s^{-1} bar^{-1}	1.65E+09	2.12E+09	2.63E+09
		k_{-6}, s^{-1} bar^{-1}	2.84E−04	2.43E−02	7.04E−01
7. (35.) $Z^-[FeOFe]^{2+}Z^-\{M=1\} + N_2O(g) \leftrightarrow Z^-[FeOFe(ON_2)]^{2+}Z^-\{M=1\}$	$\Delta H_7 = -2.6$	K_7, bar^{-1}	7.01E−05	5.02E−05	4.01E−05
	$E_7{}^{\dagger} = 0.0$	A_7, s^{-1} bar^{-1}	2.23E+07	3.14E+07	4.26E+07
		k_7, s^{-1} bar^{-1}	2.23E+07	3.14E+07	4.26E+07
	$E_{-7}{}^{\dagger} = 4.4$	A_{-7}, s^{-1}	1.25E+13	1.46E+13	1.67E+13
		k_{-7}, s^{-1}	3.18E+11	6.27E+11	1.06E+12
8. (36.) $Z^-[FeOFe(ON_2)]^{2+}Z^-\{M=1\} \leftrightarrow Z^-[FeOFeO]^{2+}Z^-\{M=1\} + N_2(g)$	$\Delta H_8 = -11.3$	K_8, bar	6.88E+08	1.79E+08	6.40E+07
	$E_8{}^{\dagger} = 24.0$	A_8, s^{-1}	1.08E+13	1.23E+13	1.38E+13
		k_8, s^{-1}	2.01E+04	4.06E+05	3.91E+06
	$E_{-8}{}^{\dagger} = 34.4$	A_{-8}, s^{-1} bar^{-1}	9.97E+07	1.25E+08	1.54E+08
		k_{-8}, s^{-1} bar^{-1}	2.92E−05	2.27E−03	6.11E−02
9. (37.) $Z^-[FeOFeO]^{2+}Z^-\{M=1\} + N_2O(g) \leftrightarrow Z^-[(N_2O)FeOFeO]^{2+}Z^-\{M=1\}$	$\Delta H_9 = -3.3$	K_9, bar^{-1}	5.77E−05	3.81E−05	2.88E−05
	$E_9{}^{\dagger} = 0.0$	A_9, s^{-1} bar^{-1}	1.11E+07	1.56E+07	2.10E+07
		k_9, s^{-1} bar^{-1}	1.11E+07	1.56E+07	2.10E+07
	$E_{-9}{}^{\dagger} = 5.0$	A_{-9}, s^{-1}	1.25E+13	1.46E+13	1.67E+13
		k_{-9}, s^{-1}	1.93E+11	4.08E+11	7.29E+11
10. (38.) $Z^-[(N_2O)FeOFeO]^{2+}Z^-\{M=1\} \leftrightarrow Z^-[OFeOFeO]^{2+}Z^-\{M=1\} + N_2(g)$	$\Delta H_{10} = -4.9$	K_{10}, bar	2.45E+06	1.38E+06	8.83E+05
	$E_{10}{}^{\dagger} = 30.1$	A_{10}, s^{-1}	2.67E+13	3.01E+13	3.33E+13
		k_{10}, s^{-1}	2.77E+02	1.16E+04	1.93E+05
	$E_{-10}{}^{\dagger} = 34.7$	A_{-10}, s^{-1} bar^{-1}	4.94E+08	5.73E+08	6.59E+08
		k_{-10}, s^{-1} bar^{-1}	1.13E−04	8.40E−03	2.18E−01
11. (39.) $Z^-[OFeOFeO]^{2+}Z^-\{M=1\} \leftrightarrow Z^-[FeOOFeO]^{2+}Z^-\{M=1\}$	$\Delta H_{11} = 9.9$	K_{11}, –	3.40E−02	1.11E−01	2.71E−01
	$E_{11}{}^{\dagger} = 31.0$	A_{11}, s^{-1}	4.01E+14	4.96E+14	5.84E+14
		k_{11}, s^{-1}	2.02E+03	1.02E+05	1.96E+06

(*continued on next page*)

Table 2 (*continued*)

Reaction[a]	$E^{\dagger}$[b], ΔH[c] (kcal/mol)	Constant	T (K)		
			600	700	800
	$E_{-11}{}^{\dagger} = 22.1$	A_{-11}, s^{-1}	6.55E+12	7.22E+12	7.79E+12
		k_{-11}, s^{-1}	5.92E+04	9.19E+05	7.22E+06
12. (40.) $Z^-[FeOOFeO]^{2+}Z^-\{M=1\} \leftrightarrow Z^-[FeO_2FeO]^{2+}Z^-\{M=1\}$	$\Delta H_{12} = -4.9$	K_{12}, –	7.23E+00	4.00E+00	2.57E+00
	$E_{12}{}^{\dagger} = 6.4$	A_{12}, s^{-1}	1.95E+12	1.84E+12	1.74E+12
		k_{12}, s^{-1}	9.40E+09	1.90E+10	3.18E+10
	$E_{-12}{}^{\dagger} = 10.6$	A_{-12}, s^{-1}	1.28E+13	1.26E+13	1.22E+13
		k_{-12}, s^{-1}	1.30E+09	4.76E+09	1.24E+10
13. (41.) $Z^-[FeO_2FeO]^{2+}Z^-\{M=1\} \leftrightarrow Z^-[FeOFeO_2]^{2+}Z^-\{M=1\}$	$\Delta H_{13} = -25.1$	K_{13}, –	1.03E+10	5.04E+08	5.25E+07
	$E_{13}{}^{\dagger} = 22.0$	A_{13}, s^{-1}	4.47E+12	4.84E+12	5.16E+12
		k_{13}, s^{-1}	4.21E+04	6.38E+05	4.92E+06
	$E_{-13}{}^{\dagger} = 47.5$	A_{-13}, s^{-1}	8.76E+11	9.07E+11	9.34E+11
		k_{-13}, s^{-1}	4.09E−06	1.27E−03	9.38E−02
14. (42.) $Z^-[FeOFeO_2]^{2+}Z^-\{M=1\} \leftrightarrow Z^-[FeOFeO_2]^{2+}Z^-\{M=3\}$	$\Delta H_{14} = -4.7$	K_{14}, –	1.57E+02	8.94E+01	5.85E+01
	$E_{14}{}^{\dagger} = 7.9$	A_{14}, s^{-1}	1.25E+13	1.46E+13	1.67E+13
		k_{14}, s^{-1}	1.67E+10	5.01E+10	1.16E+11
	$E_{-14}{}^{\dagger} = 12.6$	A_{-14}, s^{-1}	4.11E+12	4.80E+12	5.50E+12
		k_{-14}, s^{-1}	1.06E+08	5.60E+08	1.99E+09
15. (43.) $Z^-[FeOFeO_2]^{2+}Z^-\{M=3\} \leftrightarrow Z^-[FeOFe]^{2+}Z^-\{M=1\} + O_2(g)$	$\Delta H_{15} = 7.1$	K_{15}, bar	2.47E+03	6.97E+03	1.48E+04
	$E_{15}{}^{\dagger} = 8.8$	A_{15}, s^{-1}	7.03E+13	7.09E+13	7.13E+13
		k_{15}, s^{-1}	2.47E+10	7.75E+10	1.83E+11
	$E_{-15}{}^{\dagger} = 0.0$	A_{-15}, s^{-1} bar^{-1}	1.00E+07	1.11E+07	1.24E+07
		k_{-15}, s^{-1} bar^{-1}	1.00E+07	1.11E+07	1.24E+07

[a] Numbers in brackets refer to the corresponding reaction in Table 1.
[b] Calculated activation energy including zero-point energy correction.
[c] Calculated enthalpy averaged over 600–800 K.
[d] Reaction has not been described in Ref. [35].

Table 3
Norm of the gradient difference at the point of spin surface crossing and thermally averaged Landau–Zener transition probabilities at temperatures of 600, 700, and 800 K[a]

Reaction[b]	$\lvert \mathrm{grad}(E_1) - \mathrm{grad}(E_2) \rvert$ (kJ/mol/A)	P_{LZ} ($H_{12} = 395$ J/mol)			P_{LZ} ($H_{12} = 825$ J/mol)		
		T (K)			T (K)		
		600	700	800	600	700	800
Ferromagnetically coupled iron atoms							
10. $Z^-[HOFeO\_FeOH]^{2+}Z^-\{M=9\} \leftrightarrow Z^-[HOFeOFeOH]^{2+}Z^-\{M=11\}$	240	0.045	0.042	0.040	0.139	0.131	0.125
13. $Z^-[HOFeO\_OFeOH]^{2+}Z^-\{M=9\} \leftrightarrow Z^-[HOFeOOFeOH]^{2+}Z^-\{M=11\}$	158	0.066	0.062	0.059	0.196	0.185	0.177
17. $Z^-[OFeOHFeOH]^{2+}Z^-\{M=11\} \leftrightarrow Z^-[OFeOHFeOH]^{2+}Z^-\{M=9\}$	428	0.032	0.030	0.028	0.101	0.096	0.091
19. $Z^-[HOFeOHFeO]^{2+}Z^-\{M=11\} \leftrightarrow Z^-[HOFeOHFeO]^{2+}Z^-\{M=9\}$	414	0.029	0.027	0.025	0.094	0.088	0.084
42. $Z^-[FeOFeO_2]^{2+}Z^-\{M=9\} \leftrightarrow Z^-[FeOFeO_2]^{2+}Z^-\{M=11\}$	128	0.085	0.080	0.076	0.244	0.232	0.221
Antiferromagnetically coupled iron atoms							
14. $Z^-[FeOFeO_2]^{2+}Z^-\{M=1\} \leftrightarrow Z^-[FeOFeO_2]^{2+}Z^-\{M=3\}$	125	0.086	0.081	0.077	0.248	0.235	0.225

[a] Landau–Zener probabilities are calculated for a spin–orbit coupling energy of $H_{12} = 395$ and 825 J/mol.
[b] Reaction numbers are the same as those in Tables 1 and 2, respectively.

creates errors smaller than the error in the activation barrier of 5 kcal/mol at 700 K.

References

[1] D.J. Wuebbles, A. Jain, J. Edmonds, D. Harvey, K. Hayhoe, Environ. Pollution 100 (1999) 57.
[2] G.C. Rhoderick, W.D. Dorko, Environ. Sci. Technol. 38 (2004) 2685.
[3] Y. Li, J.N. Armor, Appl. Catal. B 1 (1992) L21.
[4] F. Kapteijn, J. Rodriguez-Mirasol, J.A. Moulijn, Appl. Catal. B 9 (1996) 25.
[5] J. Pérez-Ramírez, F. Kapteijn, G. Mul, X. Xu, J.A. Moulijn, Catal. Today 76 (2002) 55.
[6] J. Pérez-Ramírez, F. Kapteijn, K. Schöffel, J.A. Moulijn, Appl. Catal. B 44 (2003) 117.
[7] F. Kapteijn, G. Marbán, J. Rodriguez-Mirasol, J.A. Moulijn, J. Catal. 167 (1997) 256.
[8] T.V. Voskoboinikov, H.Y. Chen, W.M.H. Sachtler, Appl. Catal. B 19 (1998) 279.
[9] Q. Zhu, B.L. Mojet, R.A.J. Janssen, E.J.M. Hensen, J. van Grondelle, P.C.M.M. Magusin, R.A. van Santen, Catal. Lett. 81 (2002) 205.
[10] J. Pérez-Ramírez, F. Kapteijn, J.C. Groen, A. Doménech, G. Mul, J.A. Moulijn, J. Catal. 214 (2003) 33.

[11] E.V. Starokon, K.A. Dubkov, L.V. Pirutko, G.I. Panov, Top. Catal. 23 (2003) 137.
[12] P.K. Roy, G.D. Pirngruber, J. Catal. 227 (2004) 164.
[13] G.D. Pirngruber, M. Luechinger, P.K. Roy, A. Cecchetto, P. Smirniotis, J. Catal. 224 (2004) 429.
[14] B.R. Wood, J.A. Reimer, A.T. Bell, M.T. Janicke, K.C. Ott, J. Catal. 224 (2004) 148.
[15] T. Nobukawa, M. Yoshida, S. Kameoka, S. Ito, K. Tomishige, K. Kunimori, Stud. Surf. Sci. Catal. 154 (2004) 2514.
[16] L. Kiwi-Minsker, D.A. Bulushev, A. Renken, Catal. Today 91–92 (2004) 165.
[17] J.B. Taboada, A.R. Overweg, P.J. Kooyman, I.W.C.E. Arends, G. Mul, J. Catal. 231 (2005) 56.
[18] C. Sang, B.H. Kim, C.R.F. Lund, J. Phys. Chem. B 109 (2005) 2295.
[19] T. Turek, Catal. Today 105 (2005) 275.
[20] G. Berlier, G. Ricchiardi, S. Bordiga, A. Zecchina, J. Catal. 229 (2005) 127.
[21] K. Krishna, M. Makkee, Catal. Lett. 106 (2006) 183.
[22] K. Sun, H. Xia, E.J.M. Hensen, R.A. van Santen, C. Li, J. Catal. 238 (2006) 186.
[23] G.D. Pirngruber, J.D. Grunwaldt, P.K. Roy, J.A. van Bokhoven, O. Safonova, P. Glatzel, Catal. Today (2006), doi:10.1016/j.cattod.2006.09.021, in press.
[24] H.Y. Chen, W.H.M. Sachtler, Catal. Today 42 (1998) 73.
[25] El-M. El-Malki, R.A. van Santen, W.M.H. Sachtler, J. Phys. Chem. B 103 (1999) 4611.
[26] P. Marturano, L. Drozdová, G.D. Pirngruber, A. Kogelbauer, R. Prins, Phys. Chem. Chem. Phys. 3 (2001) 5585.
[27] G. Čík, M. Hubinová, F. Šeršen, V. Brezová, Collect. Czech. Chem. Commun. 67 (2002) 1743.
[28] W.M. Heijboer, Ph.D. thesis, Utrecht University, 2005.
[29] G.D. Pirngruber, P.K. Roy, R. Prins, Phys. Chem. Chem. Phys. 8 (2006) 3939.
[30] J. Pérez-Ramírez, J. Catal. 227 (2004) 512.
[31] W.M. Heijboer, D.C. Koningsberger, B.M. Weckhuysen, F.M.F. de Groot, Catal. Today 110 (2005) 228.
[32] L. Čapek, V. Kreibich, J. Dědeček, T. Grygar, B. Wichterlová, Z. Sobalík, J.A. Martens, R. Brosius, V. Tokarová, Microporous Mesoporous Mater. 80 (2005) 279.
[33] A. Heyden, B. Peters, A.T. Bell, F.J. Keil, J. Phys. Chem. B 109 (2005) 1857.
[34] A. Heyden, N. Hansen, A.T. Bell, F.J. Keil, J. Phys. Chem. B 110 (2006) 17096.
[35] N. Hansen, A. Heyden, A.T. Bell, F.J. Keil, J. Phys. Chem. C 111 (2007) 2092.
[36] L.J. Broadbelt, R.Q. Snurr, Appl. Catal. A 200 (2000) 23.
[37] A. Heyden, A.T. Bell, F.J. Keil, J. Catal. 233 (2005) 26.
[38] D.A. McQuarry, Statistical Mechanics, Harper Collins Publisher, New York, 1973.
[39] A.E. Stearn, H. Eyring, J. Chem. Phys. 3 (1935) 778.
[40] D. Danovich, S. Shaik, J. Am. Chem. Soc. 119 (1997) 1773.
[41] A. Heyden, Ph.D. thesis, Hamburg University of Technology, 2005.
[42] S.M. Rump, Ph.D. thesis, University of Karlsruhe, 1980.
[43] S.M. Rump, in: A New Approach to Scientific Computation, Academic, New York, 1983, p. 51.
[44] Numerical Algorithms Group Fortran Library, Mark 19, NAG GmbH, Garching, Routine: F07AEF.
[45] G. Emig, R. Dittmeyer, in: G. Ertl, H. Knözinger, J. Weitkamp (Eds.), Handbook of Heterogeneous Catalysis, vol. 3, Wiley–VCH, 1997, p. 1209.
[46] L. Kiwi-Minsker, D.A. Bulushev, A. Renken, Catal. Today 110 (2005) 191.
[47] E.V. Kondratenko, J. Pérez-Ramírez, J. Phys. Chem. B 110 (2006) 22586.
[48] Y. Zhao, N. González-García, D.G. Truhlar, J. Phys. Chem. A 109 (2005) 2012.